

A Comparative Study of the Turbulence-Closure Model for a FM01-LC Electrochemical Reactor

J.A Delgadillo^{*}, R. Enciso, C. Ojeda, I. Rodríguez

Facultad de Ingeniería-Instituto de Metalurgia, Universidad Autónoma de San Luis Potosí. Av. Sierra Leona 550 Lomas 2a Sec. 78210 San Luis Potosí, Mexico

*E-mail: jose.delgadillo@uaslp.mx

Received: 21 October 2011 / Accepted: 22 November 2011 / Published: 1 March 2012

In this work, a description of the dynamics in a FM01-LC electrochemical reactor was performed using computational fluid dynamics (CFD) in an attempt to characterize this reactor. A three-dimensional solution is presented using laminar and κ - ε models. The commercial software FLUENT 6.3.26 was used to solve the governing equations and predict the fluid velocity profile. The computed profiles are compared with experimental velocity profiles measured using digital image analysis (DIA) with different flow rates. The results were not satisfactory with the κ - ε model; however, the laminar modeling approach was found to describe the velocity profiles accurately.

Keywords: Computational fluid dynamics, Electrochemical reactor, Filter-press cell, Flow visualization

1. INTRODUCTION

The FM01-LC electrochemical cell is a laboratory-scale prototype of a FM21-SP cell, which is used for many electrochemical industrial applications. Characterization of the operation of an electrolytic reactor is needed to achieve optimum efficiency of the relevant process. The FM01-LC cell design is a convenient choice because of the use of parallel plates and the simple design; cell construction can be based on any type of materials. In addition, mass transport is readily controlled and simple to scale up from pilot-plant size into an industrial-scale operation.

Characterization of the fluid dynamics in a parallel-plate reactor is essential because the geometry, kinetic energy and flow of the electrolyte control the uniformity and magnitude of mass transport. However, the dynamics of the flow must be described accurately, and a description of the turbulence closure is mandatory for an acceptable characterization of the flow. Characterization of the experimental flow can be achieved through studies of the global mass transfer coefficients, local

current distributions or residence time distributions. However, the most direct approach for characterizing the experimental flow involves the evaluation of the dynamics of the flow inside the reactor. Characterization of the fluid dynamics is useful for determining which sections in the reactor contribute to inefficiencies in the process.

Nelissen et al. [1] used a residual distribution model to solve the multi-ion transport and reaction model for a turbulent flow. This model describes the effects of convection, diffusion, migration, chemical and electrode reactions of the electrolyte and potential and current density distributions in an electrochemical reactor. The authors validated different turbulence-closure models to describe the experimental results in a parallel plate reactor for the deposition of Cu from an acidic copper-plating bath. In this study, the solution is considered to be sufficiently dilute that the cross-diffusion terms and different velocities of the individual species can be neglected. The κ - ω turbulence-closure model proposed by Wilcox [2] was used in Nelissen et al. [1] study. This model does not consider the reaction to be a homogeneous one, and the effect of turbulence on mass transfer is modeled by adding the turbulent diffusion term (D_t) to the molecular diffusion. As described previously [3-6], turbulent diffusion models are used for high Schmidt numbers in mass-transfer calculations.

Vazquez et al. [7] used Fluent™ software to analyze the hydrodynamic behavior in the FM01-LC electrochemical reactor; the simulated data were then compared with experimental current distribution values obtained by Brown et al. [8]. In the former work, the authors considered a steady state flow in which the temperature and viscosity remained constant and the fluid was incompressible; in addition, natural convection was neglected, due to predominance of forced convection. Deviations from predictions at the first part of the channel suggest that local mass transport coefficients and local flow velocities follow similar behavior. Based on the described flow, the renormalization group κ - ε (RNG κ - ε) model was used to model the flow through the channel. The RNG κ - ε model is usually applied to describe flow regions that are dominated by strong velocity gradients, such as vortex flows that characterize recirculation flow regions or boundary layer separation flows [9]. The RNG κ - ε model uses the standard κ - ε model to solve the transport equations that represent the kinetic energy, κ , and its dissipation rate, ε . The formation of jets was reported for the inlet zone [7] where the strongest jets always form at the bottom of the channel, decreasing towards the top portion of the channel.

El-Behery et al. [10] compared seven turbulence models to determine the flow in a planar asymmetric diffuser. No slip boundary condition was applied along the solid walls, and standard wall functions were used. At the diffuser entrance, flat velocity and turbulence quantities profiles were specified. To obtain a reasonable solution, a second order upwind discretization scheme was used for the momentum equation, and a first order upwind discretization scheme was used for turbulent quantities. These schemes ensured accuracy, stability and convergence of the solution. The SIMPLE algorithm was employed for pressure-velocity coupling. In this case, the κ - ε and RSM models failed to predict the boundary layer separation and, consequently, the friction coefficient.

In this paper, a computational fluid dynamics (CFD) simulation of a FM01-LC electrochemical reactor is presented. Fluent™ software was used to solve the Navier-Stokes equations, and the computed results are compared with published data of flow visualization by Velasco et al. [11].

2. GOVERNING EQUATIONS

Fluid dynamics models have three main parts, including the mass balance, momentum balance and turbulence effect. The mass balance is described with the continuity equation, the momentum balance is described with the Navier-Stokes equations and the turbulence effect is described with a turbulence-closure model. The continuity equation and Navier-Stokes equations are nonlinear partial differential equations in three dimensions and thus require significant computational effort. The solutions to these equations fall under the discipline known as computational fluid dynamics (CFD).

The mass balance is described by the continuity equation shown in Equation (1).

$$\frac{\partial \rho}{\partial t} + \rho \frac{\partial u_i}{\partial x_i} = 0 \quad (1)$$

The momentum balance is described by the Navier-Stokes equations, written with index notation, as shown in Equation (2).

$$\frac{\partial(\rho u_i)}{\partial t} + \frac{\partial(\rho u_i u_j)}{\partial x_j} = -\frac{\partial \rho}{\partial x_i} + \frac{\partial}{\partial x_j} \left(\mu \frac{\partial u_i}{\partial x_j} \right) + \rho g_i \quad (2)$$

Any fluid flow can be described with Equations (1) and (2). These equations are partial differential equations and can only be solved using numerical methods. A numerical solution requires meshing of the domain. The mesh must be extremely fine to capture the smallest of the velocity fluctuations that describes the turbulence effect of the flow. A fine mesh requires significant computational time, and sometimes, obtaining a solution in a reasonable length of time is not possible even with current computing power.

The computing time can be considerably reduced when the velocity is decomposed into its mean and fluctuating components. The resulting equations for incompressible fluids are shown in Equations (3) and (4). Consequently, these equations describe the mean velocity field that can be resolved with a coarser mesh. The governing equations for the velocity field in an incompressible fluid can be written according to Equations (2) and (3) when the velocity (u_i) is described by its mean ($\langle u_i \rangle$) and fluctuation (u_i') (Equation (1)).

$$u_i = \langle u_i \rangle + u_i' \quad (3)$$

$$\frac{\partial \rho}{\partial t} + \rho \frac{\partial \langle u_i \rangle}{\partial x_i} = 0 \quad (4)$$

$$\frac{\partial(\rho\langle u_i \rangle)}{\partial t} + \frac{\partial(\rho\langle u_i \rangle\langle u_j \rangle)}{\partial x_j} = -\frac{\partial(\rho)}{\partial x_i} + \frac{\partial}{\partial x_j} \left(\mu \frac{\partial \langle u_i \rangle}{\partial x_j} \right) + \frac{\partial}{\partial x_j} (-\rho\langle u_i u_j \rangle) + \rho g_i \quad (5)$$

Here, the term $-\rho\langle u_i u_j \rangle$ includes the turbulence effect, which must be modeled to close Equation (5). There are different models used to describe this term. Among the available turbulence models, the κ - ε model has been applied with a degree of success in a wide number of geometries. However, the flow may be laminar, and the turbulence term is not significant. Therefore, a comparison between laminar and κ - ε models is presented.

2.1 The κ - ε model

The κ - ε model is simple to apply, and this model can describe the turbulence effect for most engineering flow problems. The κ - ε model is a semiempirical model, and derivation of the model equations relies on phenomenological considerations and empiricism [12]. The standard κ - ε model is based on model transport equations for the turbulence kinetic energy (κ) and its dissipation rate (ε). The main assumption in the derivation for the κ - ε model is that the flow is fully turbulent, and the molecular viscosity effect is negligible. Thus, the standard κ - ε model is valid only for fully turbulent flows. A description of the turbulence kinetic energy, κ , is obtained using equation (6), and the dissipation rate, ε , is obtained using equation (7).

$$\frac{\partial}{\partial t}(\rho k) + \frac{\partial}{\partial x_i}(\rho k u_i) = \frac{\partial}{\partial x_j} \left[\left(\mu + \frac{\mu_t}{\sigma_k} \right) \frac{\partial k}{\partial x_j} \right] + G_k + G_b - \rho \varepsilon - Y_M + S_k \quad (6)$$

$$\frac{\partial}{\partial t}(\rho \varepsilon) + \frac{\partial}{\partial x_i}(\rho \varepsilon u_i) = \frac{\partial}{\partial x_j} \left[\left(\mu + \frac{\mu_t}{\sigma_\varepsilon} \right) \frac{\partial \varepsilon}{\partial x_j} \right] + C_{1\varepsilon} \frac{\varepsilon}{k} (G_k + C_{3\varepsilon} G_b) - C_{2\varepsilon} \rho \frac{\varepsilon^2}{k} + S_\varepsilon \quad (7)$$

In these equations, G_k represents the generation of turbulence kinetic energy due to the mean velocity gradients, G_b represents the turbulence kinetic energy generated by buoyancy and Y_M represents the contribution of the fluctuating dilatation in compressible turbulence to the overall dissipation rate. $C_{1\varepsilon}$, $C_{2\varepsilon}$ and $C_{3\varepsilon}$, are constants. σ_k and σ_ε are the Prandtl turbulent numbers for k and ε , respectively, and S_k and S_ε are user-defined source terms.

The turbulent (or eddy) viscosity, μ_t , is calculated by combining κ and ε , as shown in equation 8 in which C_μ is a constant.

$$\mu_t = \rho C_\mu \frac{k^2}{\varepsilon} \quad (8)$$

The model constants $C_{1\varepsilon}$, $C_{2\varepsilon}$, C_μ , σ_k and σ_ε have default values of 1.44, 1.92, 0.09, 1.0 and 1.3, respectively.

These default values were measured from experiments with air and water to determine fundamental turbulent shear flows, including shear flows and decaying isotropic grid turbulence. These values work relatively well for a wide range of wall-bounded and free shear flows. The $C_{3\varepsilon}$ term is not included because water is the fluid being used.

3. EXPERIMENTAL DATA

Published experimental data [11] were used to validate the simulated results. The inlet flow rate was changed to three different levels: $0.0631 \text{ L min}^{-1}$, 0.315 L min^{-1} and 0.631 L min^{-1} . A Canon GL 3CCD NTSC video camera was used to record slow-motion videos at the three flow conditions. A high intensity illumination source was used to capture videos with a speed of $1/2400 \text{ s}$. The video was sectioned into frames to calculate fluid velocity using an ink tracer.

The captured video is formed by a finite number of images; thus, it can be transformed into a sequence of timed frames. The time between frames and the positions of the colored fluid before and after each frame are known. The instantaneous velocity can be calculated from these known values. These measurements are accurate if the time between frames is small enough to obtain a good approximation of an instant velocity. Natural diffusion of the ink into the fluid will occur, but this problem is minimized using high-molecular-weight inks. The images generated from the videos were analyzed with the open-source software ImageJ. ImageJ calculates fluid displacement between frames during a known time period. Using this methodology, experimental velocity profiles at a distance of 80 mm from the chamber inlet were generated using videos obtained from Velasco et al. [11]. The experimental velocity profiles were compared with the simulated data using turbulent and laminar approaches to evaluate the fluid flow.

3.1 Determination of the experimental velocity profiles

Three flow rates were analyzed, and experimental velocity profiles were calculated using digital image analysis (DIA). Figure 1 shows the asymmetrical distribution of the flow rate at $0.0631 \text{ L min}^{-1}$ for different time frames. At this flow rate, the inlet Reynolds number (Re) is 45. There is a clear velocity gradient on the vertical axis; this observation deviates from the expected flat profiles generated with turbulent flows. The experimental velocity profiles were measured at a distance of 80 mm from the chamber inlet, as shown in Figure 2.

The second set of experimental velocity profiles were measured at a flow rate of 0.315 L min^{-1} (Re = 226) (Figure 2). The increase in the flow rate produces a clear alteration in the flow velocity gradient. Figure 3 shows that a higher velocity gradient is present at this flow rate with a low velocity region at the center.

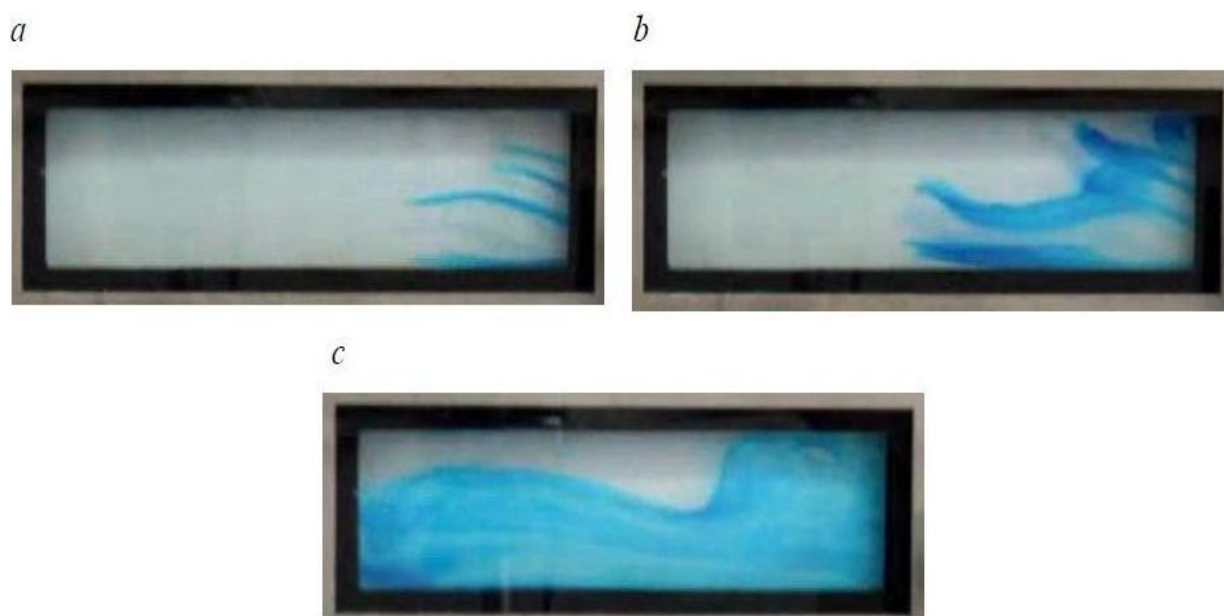


Figure 1. Video frame shots at: a) 7 s, b) 10 s and c) 18 s, with a flow rate of $0.0631 \text{ L min}^{-1}$ ($Re = 45$), obtained from Velasco et al. [11].

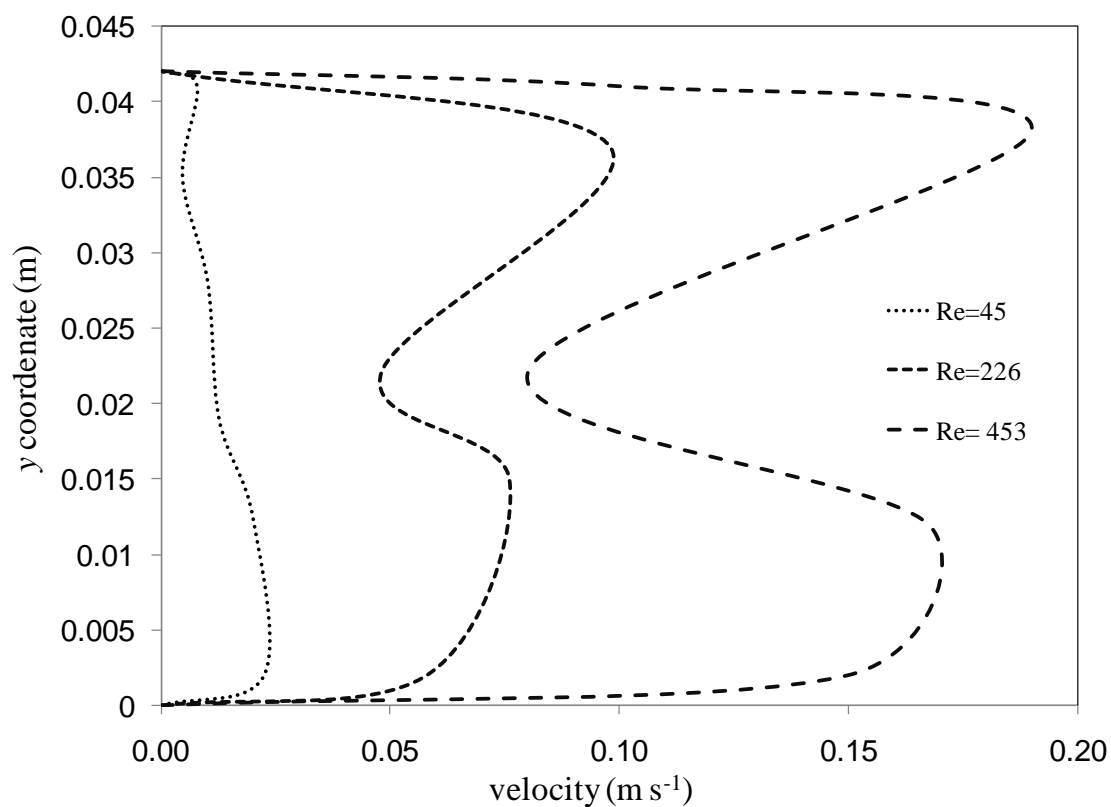


Figure 2. Calculated experimental profiles using DIA.

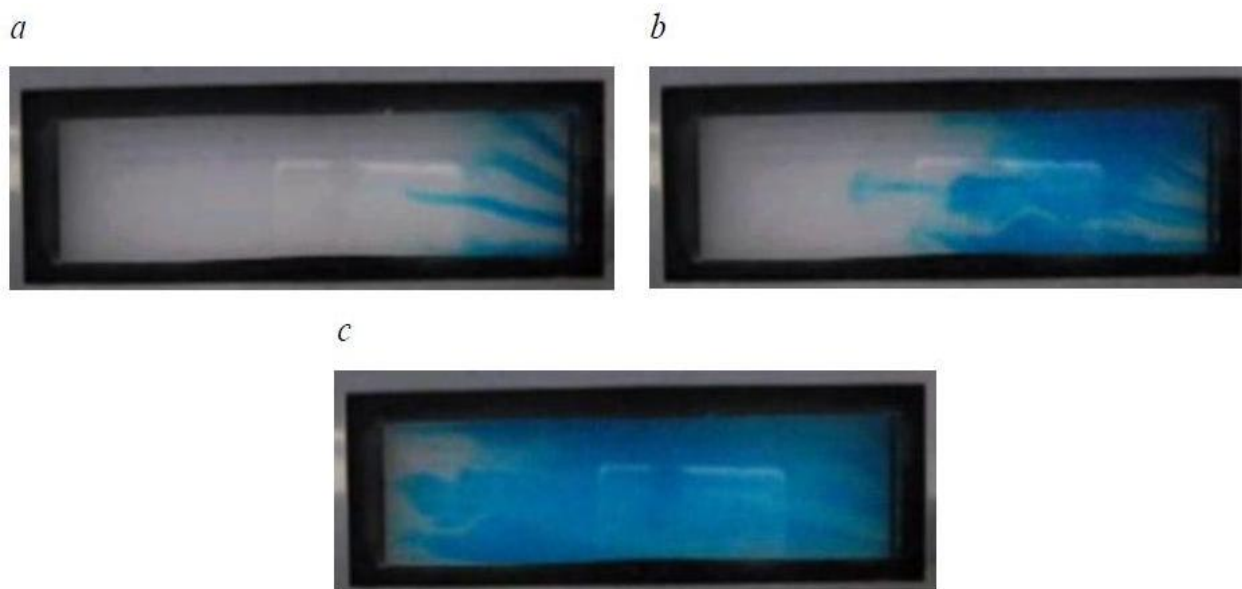


Figure 3. Video frame shots at: a) 2 s, b) 3 s and c) 5 s, with a flow rate of 0.315 L min^{-1} ($\text{Re} = 226$), obtained from Velasco et al. [11].

When the flow rate is further increased to 0.631 L min^{-1} ($\text{Re} = 453$), the frame shots exhibit a uniform flow velocity profile with a low velocity zone in the middle section of the reaction chamber that remains throughout the channel. An inspection of the video frames (Fig. 4) shows that an increase in turbulence occurs, but it is not possible to determine whether the flow has become turbulent. However, the application of the DIA methodology to analyze the images allows obtaining velocity profiles information as shown in Figure 2.

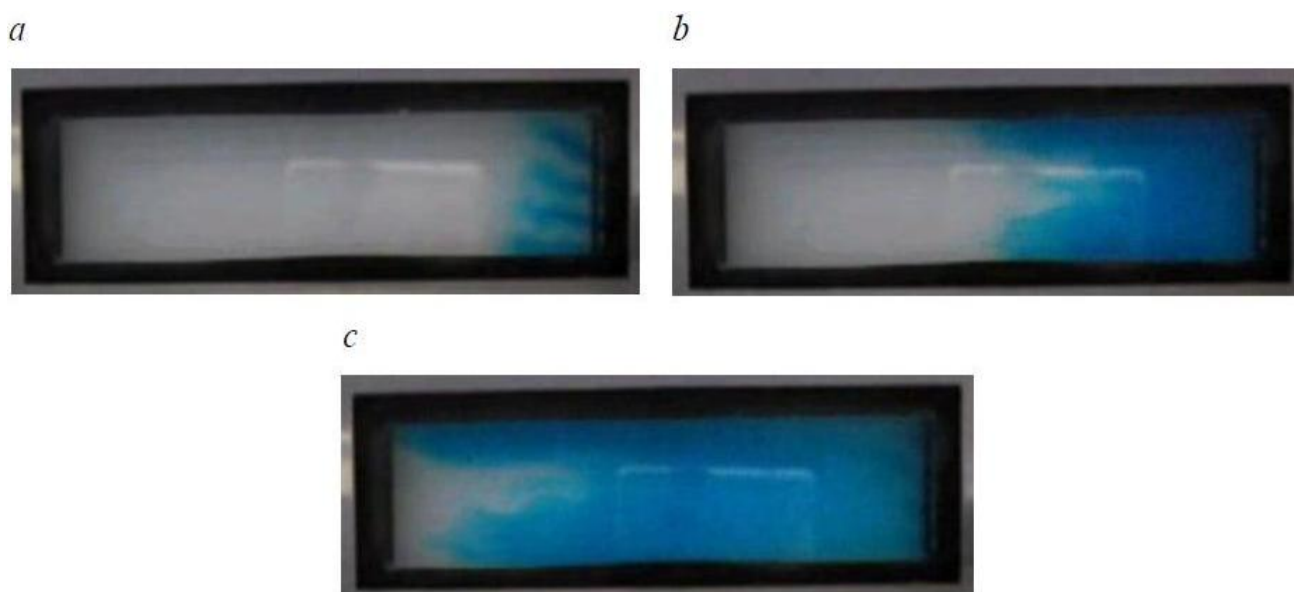


Figure 4. Video frame shots at: a) 1 s, b) 2 s and c) 3 s, with a flow rate of 0.631 L min^{-1} ($\text{Re} = 453$), obtained from Velasco et al. [11].

4. SIMULATED RESULTS

The simulated domain corresponds to the electrochemical reactor used by Velasco et al. [11]. The detailed domain geometry is shown in Figure 5. The feed and outlet are formed by five channels with average widths of 5 ± 0.5 mm. The channel lengths vary from 10 to 31.9 mm, and the diffuser chamber is 160 mm x 42 mm x 3 mm. The reactor mesh of the domain is shown in Figure 6; the mesh was divided into six sections to create a structured mesh in the reaction chamber.

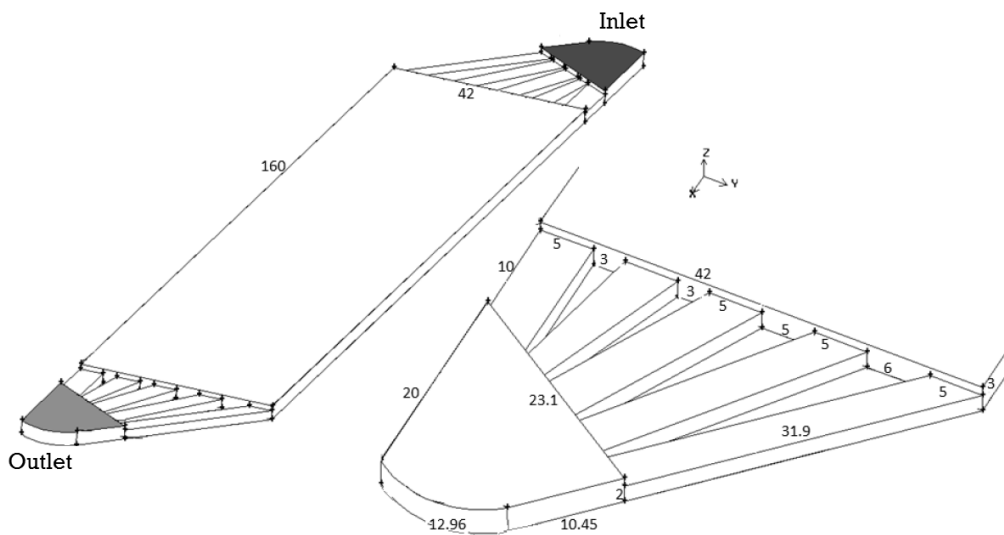


Figure 5. Detailed geometry of the simulated domain.

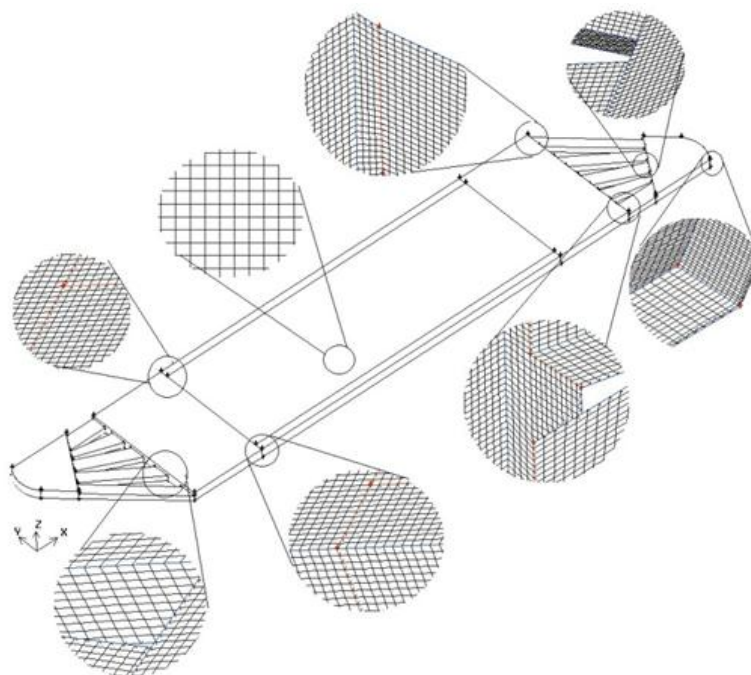


Figure 6. Domain mesh used in the simulations.

The structured hexahedral mesh (0.025 mm) starts with the inlet and outlet sections, proceeds within the channels and ends in the reaction chamber. This procedure results in improved adjustment of the shape and volume of the mesh, such that 97% of the 2,039,370 cells are hexahedral. These calculations were performed using FLUENT™ 6.3.26 with an Intel® Core™2 Duo CPU T 5770 a 2.00 GHz processor and 2 GB of RAM.

The solver was designed to be segregated, implicit and steady, and the velocity formulation was absolute. Laminar and κ - ε models were used to calculate the flow dynamics with standard wall functions. The turbulence boundary condition at the inlet and outlet was set at 10% intensity with a length scale of 0.001 m.

The simulated velocity profiles were recorded at the middle section of the reaction chamber (80 mm from the inlet) after the solution converged. Laminar and κ - ε model results were compared with the experimental velocity profiles.

The simulated results for a flow rate of 0.0631 L min⁻¹ using both models are shown in Figure 7. The simulation using the laminar model shows behavior that is consistent with the results of the experimental velocity profiles, whereas the simulation using the κ - ε model deviates from the experimental data.

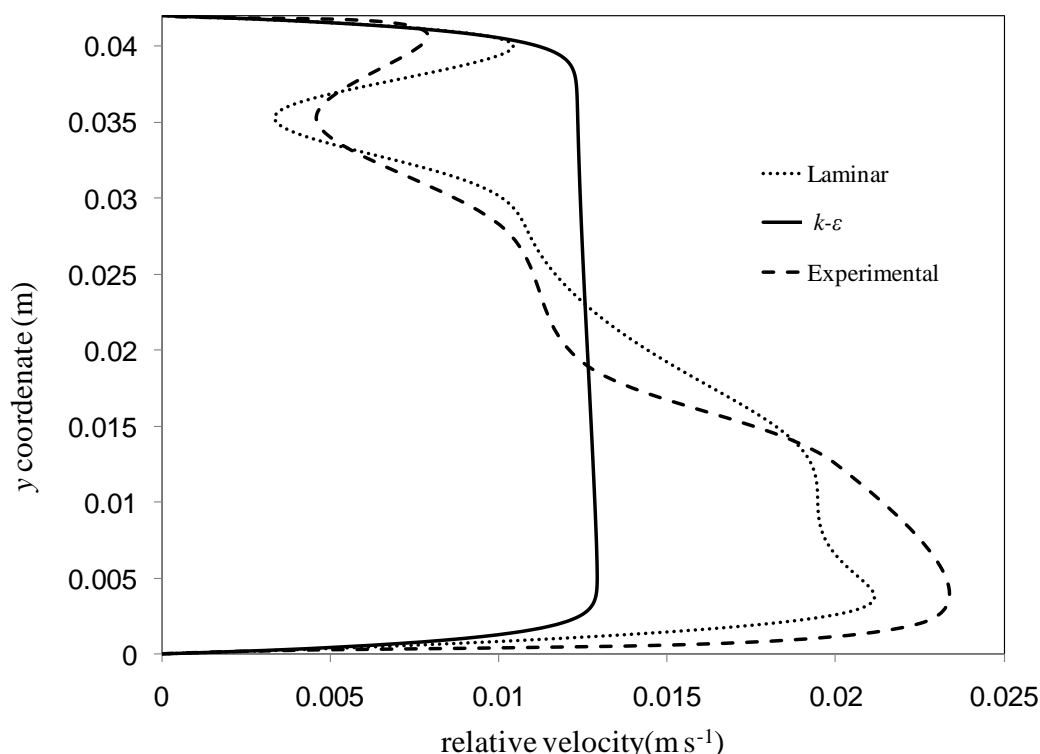


Figure 7. Simulated velocity profiles for a mass flow rate of 0.0631 L min⁻¹ (Re = 45).

Simulated results obtained for a flow rate of 0.315 L min⁻¹ using both models (Fig. 8) show that the velocity profiles for the laminar model are more consistent with the experimental results. The jet

stream at the top of the reaction chamber is clearly captured. The $\kappa\text{-}\epsilon$ model predicts a flat profile that is characteristic of a turbulent flow; therefore, the $\kappa\text{-}\epsilon$ approach cannot satisfactorily describe this flow.

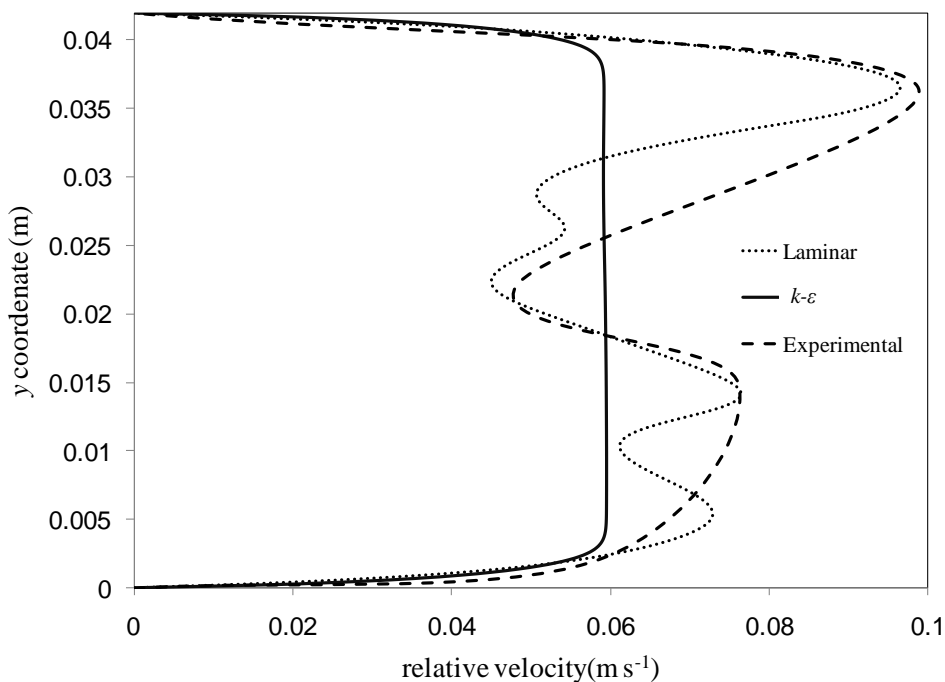


Figure 8. Simulated velocity profiles for a mass flow rate of 0.315 L min^{-1} ($\text{Re} = 226$).

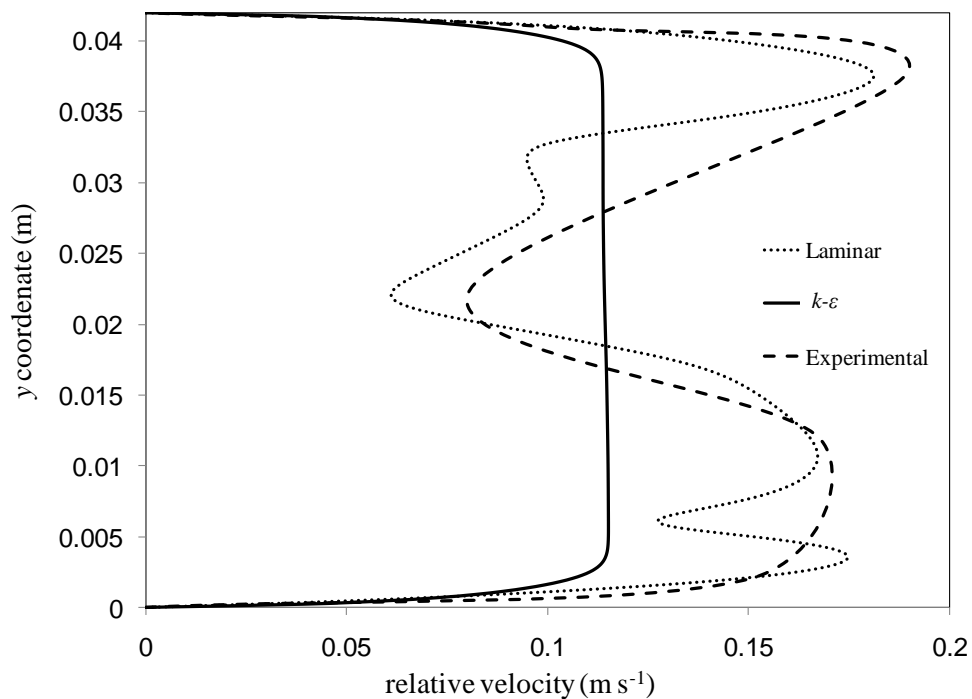


Figure 9. Simulated velocity profiles for a mass flow rate of 0.631 L min^{-1} ($\text{Re} = 453$).

Simulated results for a flow rate of 0.613 L min^{-1} (Fig. 9) also show that the laminar model is more consistent with the experimental results. Velocity profiles indicate that a low velocity zone is present in the middle of the reaction chamber; this low velocity zone appears in the three simulated flows using the laminar model but does not appear in the simulations using the $\kappa\text{-}\varepsilon$ model.

4. CONCLUSIONS

The experimental evidence reported by Velasco et al. [11] provides a qualitative description of the flow using frame shots of fluid flow videos. This approach describes the tendency of the flow, but this data is difficult to use as a validation method for CFD simulations. In this study, digital image analysis of the videos was used as a tool to determine the velocity profile of the flow at the middle of the reaction chamber. The video information was extracted, and a quantitative comparison was performed with the simulated data.

The flow conditions show that laminar flow is expected at a low Reynolds (Re) number. However, this assumption is not valid at the connecting channels, where the Reynolds number is much higher. The inlet channels create a perturbation of the flow, generating fast flow jets in different zones of the chamber, depending on the flow rate. Computational fluid dynamics calculations successfully predict the flow dynamics at different Reynolds numbers. When the turbulence intensity is low, the $\kappa\text{-}\varepsilon$ model predicts the expected flat profiles, whereas the laminar approach captures the modifications of the flow velocity gradients.

ACKNOWLEDGMENTS

The authors are grateful for financial support from PROMEP under Grant PROMEP/103.5/09/4244 and from scholarship 247934, which was provided to R. Enciso to pursue master's studies.

References

1. G. Nelissen, A. Van Theemsche, C. Dan, B. Van den Bossche, *J. Electroanal. Chem.* 563 (2004) , 213-220.
2. D.C. Wilcox, *Turbulence Modelling for CFD*, second ed., DCW Industries,. La Canada,CA, 1998.
3. F. Gurniki, S. Zahrai, F.H. Bark, *J. Appl. Electrochem.* 29 (1999) 27-34.
4. F. Gurniki, K. Fukagata, S. Zahrai, F. Bark, *J. Appl. Electrochem.* 30 (2000) 1335-1343.
5. R. Chalupa, V. Chen, A. Modi, J. West, *Int. J. Heat Mass Transfer* 44 (2001) 3775.
6. R. Chalupa, M. Chen, V. Modi, A. West, *J. Electrochem. Soc.* 148 (2001) E92-E96
7. L. Vázquez, A. Alvarez-Gallegos, F. Sierra, C. Ponce de León, F. Walsh, *Electrochim. Acta* 55 (2009) 3437-3445.
8. C. Brown, D. Pletcher, F. Walsh, J. Hammond, *J. Appl. Electrochem.* 23 (1993) 38-43
9. J.A. Delgadillo, R. Rajamani, *Int. J. Miner. Process* 77 (2005) 217-230.
10. S.M. El-Behery, M.H. Hamed, *WASET Journal* 53 (2009) 769-780
11. G. Velasco-Martinez, S. Gutierrez-Granados, A. Alatorre-Ordaz, I. Rodríguez-Torres, *ECS Trans.* 602 (2006) 1-12

12. B.E. Launder, D.B. Spalding, Lectures in Mathematical Models of Turbulence, Academic Press, London, England , 1972.